

A Counting Data Acquisition System for Measuring Parity Violation Asymmetry in Deep Inelastic Scattering

R. Subedi ^{a 1} D. Wang ^a K. Pan ^b X. Deng ^a R. Michaels ^c
P. E. Reimer ^d A. Shahinyan ^e B. Wojtsekhowski ^c X. Zheng ^{a,*}

^a*University of Virginia, Charlottesville, VA 22904, USA*

^b*Massachusetts Institute of Technology, Cambridge, MA 02139, USA*

^c*Thomas Jefferson National Accelerator Facility, Newport News, VA 23606, USA*

^d*Argonne National Laboratory, Argonne, IL 60439, USA*

^e*Yerevan Physics Institute, Yerevan, Armenia*

Abstract

An experiment measuring the parity violating asymmetry in deep inelastic scattering was completed at the Thomas Jefferson National Accelerator Facility in experimental Hall A. From this asymmetry one can extract a combination of the quark weak axial charge with a factor of five improvement in precision over world data. To achieve this, asymmetries at the 10^{-4} level were measured. A highly specialized data acquisition (DAQ) system with intrinsic particle identification (PID) was developed and utilized. The DAQ system of this experiment is presented here with an emphasis on understanding of its PID performance, deadtime effect, and the capability of measuring small asymmetries.

Key words: Jefferson Lab; Hall A; PVDIS; DAQ

PACS: 11.30.Er, 12.15.Mm, 13.60.Hb 14.60.Cd 14.65.Bt 29.30.Aj 29.85.Ca

¹ Present address: George Washington University, 725 21st St, NW, Washington, DC 20052, USA

* Corresponding author. E-mail: xiaochao@jlab.org; Telephone: 001-434-243-4032; Fax: 001-434-924-4576

22 1 Introduction

23 The Parity Violating Deep Inelastic Scattering (PVDIS) experiment E08-011 was
 24 completed in December 2009 at the Thomas Jefferson National Accelerator Facility
 25 (JLab). The goal of this experiment [1,2] is to measure to a high precision the parity
 26 violating asymmetry in deep inelastic scattering of a polarized electron beam on an
 27 unpolarized liquid deuterium target. This asymmetry is sensitive to a combination
 28 of the quark weak axial charge $2C_{2u} - C_{2d}$, where $C_{2q} = 2g_V^e g_A^q$ with $q = u, d$
 29 indicating an up or a down quark, g_V^e is the electron vector coupling and g_A^q is the
 30 quark axial coupling to the Z^0 boson.

31 For electron inclusive scattering from an unpolarized target, the electromagnetic
 32 interaction is parity conserving and is insensitive to the spin flip of the incoming
 33 electron beam. Only the weak interaction violates parity. Taking the difference of
 34 the left-handed and right-handed electron scattering cross-sections, one can isolate
 35 the parity violating contribution. The parity violating asymmetry for deep inelastic
 36 electron scattering from a deuterium target, A_{PV} , can be written as

$$A_{PV} \equiv \frac{\sigma_R - \sigma_L}{\sigma_R + \sigma_L} = \left(-\frac{G_F Q^2}{4\sqrt{2}\pi\alpha} \right) \left(2g_A^e Y_1 \frac{F_1^{\gamma Z}}{F_1^\gamma} + g_V^e Y_3 \frac{F_3^{\gamma Z}}{F_1^\gamma} \right), \quad (1)$$

37 where $\sigma_R(L)$ is the cross section for right(left) handed incident electrons, Q^2 is the
 38 negative of the four-momentum transfer squared, G_F is the Fermi weak coupling
 39 constant, α is the fine structure constant, Y_1 and Y_3 are kinematic factors, and x is
 40 the Bjorken scaling variable. In the quark parton model,

$$F_1^{\gamma Z} = \sum g_V^q Q_q [q(x) + \bar{q}(x)] \quad (2)$$

$$F_3^{\gamma Z} = \sum g_A^q Q_q [q(x) - \bar{q}(x)] \quad (3)$$

$$F_1^\gamma = \frac{1}{2} \sum Q_q^2 [q(x) + \bar{q}(x)] \quad (4)$$

41 where Q_q is the electric charge of quarks and $q(x)$, $\bar{q}(x)$ are quark distribution
 42 functions. Rewriting $g_{A(V)}^e g_{V(A)}^q$ as $C_{1(2)q}$, and assuming $R^\gamma = R^{\gamma Z} = 0$ where
 43 $R^{\gamma(Z)} = \sigma_L^{\gamma(Z)} / \sigma_T^{\gamma(Z)}$ is the ratio of the longitudinal to transverse cross section of
 44 the virtual photon exchange ($\gamma^* - Z$ interference), one has $Y_1 = 1$ and

$$A_{PV} = \left(\frac{3G_F Q^2}{\pi\alpha^2\sqrt{2}} \right) \times \frac{2C_{1u}[1 + R_C(x)] - C_{1d}[1 + R_S(x)] + Y_3(2C_{2u} - C_{2d})R_V(x)}{5 + R_S(x) + 4R_C(x)}, \quad (5)$$

45 where $R_{V,C,S}$ are related to quark distributions. The magnitude of the asymmetry

is in the order of 10^{-4} , or 10^2 parts per million (ppm) at $Q^2 = 1$ (GeV/c)². The tree-level Standard Model effective weak coupling constants $C_{1,2q}$ are

$$C_{1u} = 2g_A^e g_V^u = -\frac{1}{2} + \frac{3}{4} \sin^2 \theta_W, \quad C_{2u} = 2g_V^e g_A^u = -\frac{1}{2} + 2 \sin^2 \theta_W, \\ C_{1d} = 2g_A^e g_V^d = \frac{1}{2} - \frac{2}{3} \sin^2 \theta_W, \quad C_{2d} = 2g_V^e g_A^d = \frac{1}{2} - 2 \sin^2 \theta_W,$$

with θ_W the weak mixing angle. The goal of JLab E08-011 is to measure the PVDIS asymmetries to statistical precisions of 3% and 4% at $Q^2 = 1.1 \text{ GeV}^2$ and 1.9 GeV^2 , respectively. In addition, the systematic uncertainty goal is $< 3\%$, and under the assumption that hadronic physics corrections are small, our goal is to extract from these asymmetries the effective coupling constant combination $(2C_{2u} - C_{2d})$. The magnitude of the asymmetries is expected to be 90 and 170 ppm for the two measured kinematics of $Q^2 = 1.1$ and 1.9 (GeV/c)², respectively. To achieve the required precision, event rates up to 500 kHz are expected. Although this is not the first time the PVDIS asymmetries are measured, the only preceding PVDIS measurement was carried out at SLAC [5,6] in the late 1980's, with a $\approx 9\%$ statistical and a $\approx 9\%$ systematic uncertainties. The increased precision of this experiment required better controls of all systematic uncertainties.

The experiment used a 100 μA polarized electron beam with a polarization of approximately 90% and a 20-cm long liquid deuterium target. The two High Resolution Spectrometers (HRS) [3] were used to detect scattered electrons. Similar to other deep inelastic scattering experiments, the main challenge of the measurement is to separate electrons from charged pion background due to electro- or photo-productions. While the standard HRS detector package and data acquisition (DAQ) system routinely provide a high particle identification (PID) performance, they are based on full recording of the detector signals and are limited to event rates up to 4 kHz. This is not sufficient for the high rates expected for the experiment. The HRS DAQ will be referred to as “standard DAQ” hereafter. For previous JLab parity violation experiments [7,8] focusing on elastic scattering from nuclear or nucleon targets, integrating DAQ could be used because elastic scattering typically is not contaminated by backgrounds. For the SLAC PVDIS experiment, an integrating DAQ was used with the input being the lead-glass detector signals. However, about 2% of the integrated signal was from the pion background. This is comparable to our statistical uncertainty and a better data collection method must be found.

2 DAQ Overview

The design goal of the new DAQ is to count event rates up to 1 MHz with hardware-based PID. The following detectors in the HRS were used: two scintillator planes provided the main trigger, while a CO₂ gas cherenkov counter and a double-layered

80 lead-glass detector provided particle identification information. The standard track-
81 ing detector (the vertical drift chamber) was turned off during production data tak-
82 ing because it may not endure the expected high event rates.

83 For the gas cherenkov detector and the double-layered lead-glass counter, a full
84 recording of their output ADC spectrum is not feasible at the expected high rate.
85 Instead their signals are passed through discriminators and logic units to form pre-
86 liminary electron and pion triggers. Particle identification is fulfilled by the use of
87 discriminators for both the lead-glass and the cherenkov counters and proper set-
88 tings of their thresholds. These preliminary triggers are then combined with the
89 scintillator triggers and cherenkov signals to form the final electron and pion trig-
90 gers, which are then sent to scalers to record the event counts and form asymmetries
91 $A = (n_R - n_L) / (n_R + n_L)$, where $n_{R(L)}$ is the integrated rate of the triggers normal-
92 ized to the beam charge for the right(*R*) and left(*L*) handed spin states (helicity)
93 of the incident electron beam. The scalers that count triggers and beam charge are
94 integrated over the helicity period, which was flipped pseudo-randomly at 30 Hz
95 per the experimental technique used by the HAPPEX experiments [9].

96 For HRS the two layers of the lead-glass counter are called “preshower” and “shower”
97 detectors, respectively. The preshower blocks in the Right HRS (the spectrometer
98 located to the right side of the beamline when viewed along the beam direction)
99 has 48 blocks arranged in a 2×24 array, with the longest dimension of the blocks
100 aligned perpendicular to the particle trajectory. For the two blocks in each row,
101 only the ends facing outward are read out by photo-multiplier tubes (PMTs) and
102 the other ends of the two blocks were facing each other and not read out. Therefore
103 the preshower detector had 48 output channels. All preshower blocks were indi-
104 vidually wrapped to prevent light leak. The preshower and the shower detectors in
105 the Left HRS are similar to the preshower detector on the Right HRS except that
106 for each detector there are 34 blocks arranged in a 2×17 array. The shower de-
107 tector in the Right HRS had 75 blocks arranged in a 5×15 array with the longest
108 dimension of the blocks aligned along the trajectory of scattered particles. PMTs
109 are attached to each block of the Right shower detector on one end only, giving 75
110 output channels.

111 In order to reduce the amount of electronics needed and to avoid high electronic
112 background, the lead-glass blocks in both the preshower and the shower detectors
113 were divided into 6 (8) groups for the Left (Right) HRS, with each group consist-
114 ing 8 blocks. On the Right HRS only 60 of the 75 shower blocks were used while
115 the 15 blocks on the edge were not included in the DAQ. The reduction on the
116 HRS acceptance due to not using these side blocks is negligible. Signals from the 8
117 blocks in each group were added using a custom-made analog summing unit called
118 “SUM8 modules”, then passed to discriminators. The geometry and the position of
119 each pre-shower group was carefully chosen to match those of the corresponding
120 shower group to maximize electron detection efficiency. On the Left HRS adjacent
121 groups in both preshower and shower had overlapping blocks, while for the Right

122 HRS only preshower blocks were overlapping. To allow overlapping between ad-
 123 jacent groups, signals from preshower blocks on the Right HRS and from both
 124 preshower and shower blocks on the Left HRS were split into two identical copies
 125 using passive splitters. Grouping of the lead-glass blocks is shown in Fig. 1.

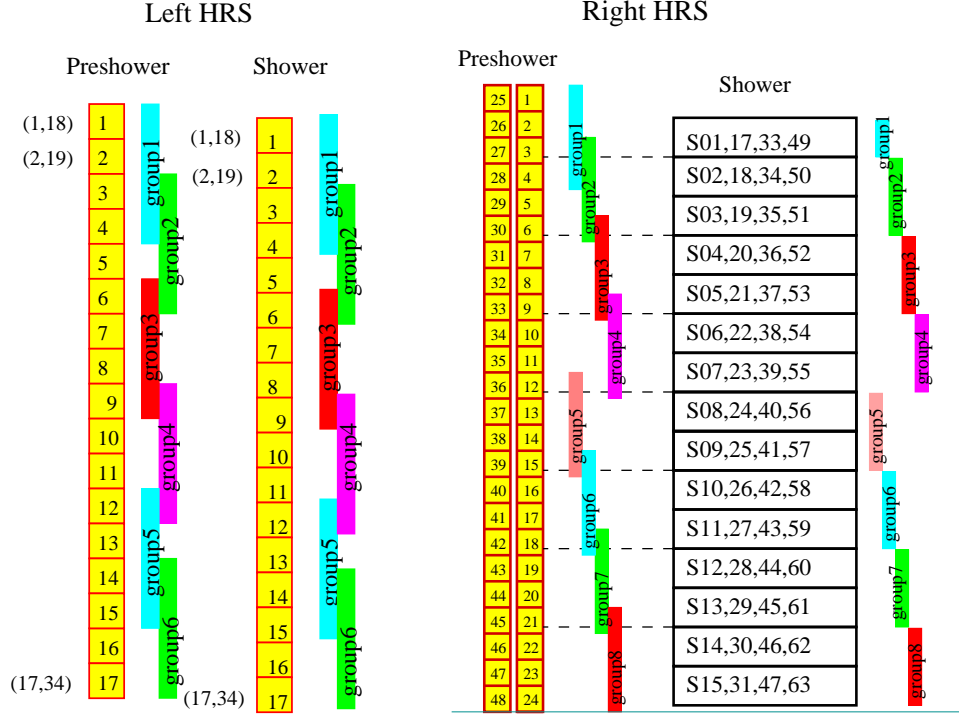


Fig. 1. [Color online] Grouping scheme (side-view) for the double-layered lead-glass counters for the Left and the Right HRS. Scattered particles enter the detector from the left. The colored vertical bars represent the range of each group.

126 A schematic diagram for the DAQ electronics for the Right HRS is shown in Fig. 2.
 127 The electron and pion triggers were formed by passing shower (SS) and preshower
 128 (PS) signals or their sums, called total shower (TS) signals, through discriminators
 129 with different thresholds. For electron triggers, logical ANDs of the preshower dis-
 130 criminator and the total shower discriminator outputs were used. For pion triggers,
 131 low threshold discriminators on the total shower signal alone were used to reject
 132 background. These signals were then combined with signals from scintillators and
 133 the gas cherenkov (called electron or pion “VETO” signals) to form electron or pion
 134 triggers for each shower and preshower group. The electron VETO signals required
 135 the gas cherenkov to be triggered, while the pion VETO required the opposite. The
 136 electron or pion triggers from all six groups on the Left HRS (eight groups for the
 137 Right HRS) were then ORed together to form the global electron or pion triggers
 138 for the Left (Right) HRS. All triggers – electron and pions from each group, as well
 139 as the final global triggers – were counted using scalars.

140 In order to study the counting deadtime of the DAQ, two identical paths of elec-
 141 tronics were constructed. The only difference between the two paths is in the dis-
 142 criminator output width, set at 30 ns and 100 ns for the narrow and the wide paths,

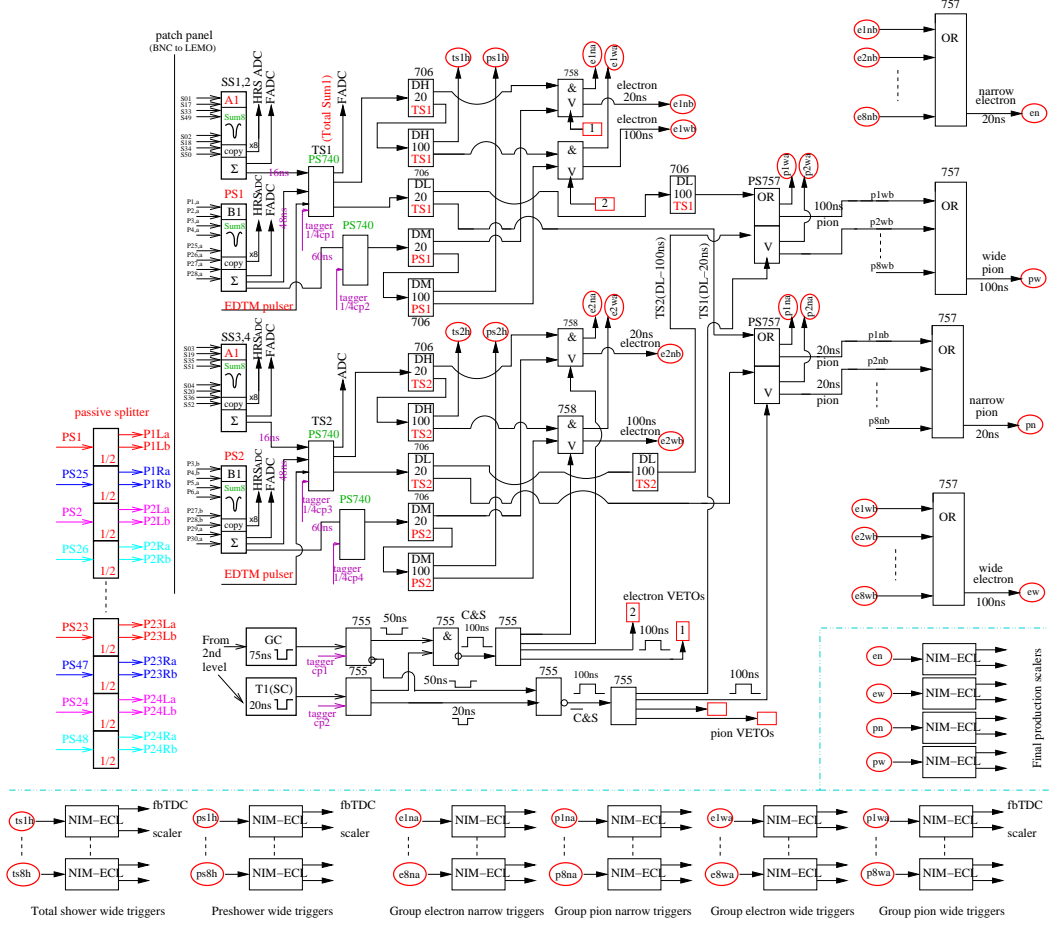


Fig. 2. [Color online] Electronics diagram for the Right HRS DAQ used by the PVDIS experiment. The Sum8's, discriminators and logic modules for two groups are shown, as well as the location of tagger signal inputs, setup of the VETO circuit using scintillator and gas cherenkov signals, the logic units for combining triggers from all eight groups into final triggers, and the scalers. Electronics for the Left HRS are similar except for the grouping scheme.

143 respectively. The scalers are rated for 250 MHz (4 ns deadtime) and therefore do
 144 not add to the deadtime. In addition, since the output width of all logic modules
 145 were set to 15 ns, the deadtime of the DAQ for each group is dominated by the
 146 deadtime of the discriminators.

147 The SUM8 modules used for summing all lead-glass signals also served as fan-
 148 out modules, providing exact copies of the input PMT signals. These copies were
 149 sent to the standard HRS DAQ, hence the standard DAQ remained fully functional.
 150 During the experiment, data were collected at low rates using reduced beam cur-
 151 rents with both DAQs functioning, such that a direct comparison of the two DAQs
 152 can be made. The vertical drift chambers were used during these low rate DAQ
 153 studies. Outputs from all discriminators, signals from the scintillator and the gas
 154 cherenkov, and all electron and pion triggers were sent to fastbus TDCs (fbTDC)
 155 and were recorded in the standard DAQ. Data from these fbTDCs were used to

align signals in timing before and throughout the experiment. They also allow the study of the cherenkov or lead-glass performance for the new DAQ triggers.

Full sampling of analog signals were done using Flash-ADCs (FADCs) at low rates intermittently during the experiment. For one group on the left and one group on the right HRS, the preshower and shower SUM8 outputs, the intermediate logical signals of the DAQ, and the output electron and pion triggers were recorded. These FADC data provided the following information: (i) They provide a study of pileup effects to confirm the simulation; (ii) They provide input parameters for the simulation, specifically the rise and fall times of the signals and their widths.

3 DAQ PID performance

PID performance of the DAQ system were studied at low beam currents using fbTDC signals along with ADC spectrum of all detector signals recorded by the standard DAQ. Figure 3 shows the preshower vs. shower signals for group 2 on the Left HRS. A comparison between no fbTDC cut and with cut on the fbTDC signal of the electron wide trigger from this group clearly shows the hardware PID cuts.

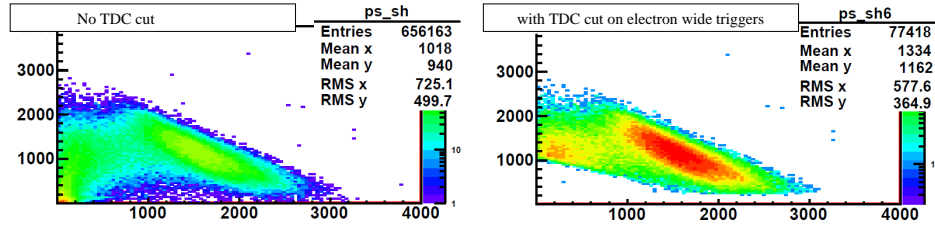


Fig. 3. [Color online] Preshower vs. Shower ADC spectrum (sum of 8 blocks each) for group 2 on the Left HRS, without fbTDC cut (left) and with cut on the group 2 electron wide trigger fbTDC signal (right). It clearly shows the hardware cuts on the preshower and the total shower signals, indicating the DAQ is selecting the correct events as electrons. The cuts can be adjusted by changing the discriminator thresholds. The events near the vertical axis, around ADC channels (200,1000), are electrons that deposited energy in overlapping blocks between group 2 and group 1 (or group 3) and are recorded by the other group.

Electron efficiency and pion rejection factors of the lead-glass counter on the Left HRS are shown in Fig. 4 as functions of the vertical hit position of the particle in the preshower detector. PID performance on the Right HRS is similar. Electron efficiency from wide groups are slightly higher than narrow groups because there is less event loss due to timing mis-alignment when taking the coincidence between the preshower and the total shower discriminator outputs. Variations in the electron efficiency across the spectrometer acceptance effectively change the kinematics (Q^2) of the measurement. For this reason, data were taken daily during the experiment to monitor the DAQ PID performance and corrections are applied to data.

181 Combined with the ≈ 200 pion rejection factor of the gas cherenkov counter, the
 182 total pion rejection achieved during this experiment was above 10^4 . With the parity
 183 violation asymmetry of pion production being no larger than that of scattered elec-
 184 trons, the uncertainty in the final asymmetry results due to pion contamination is
 185 negligible compared to the 3 – 4% statistical uncertainty.

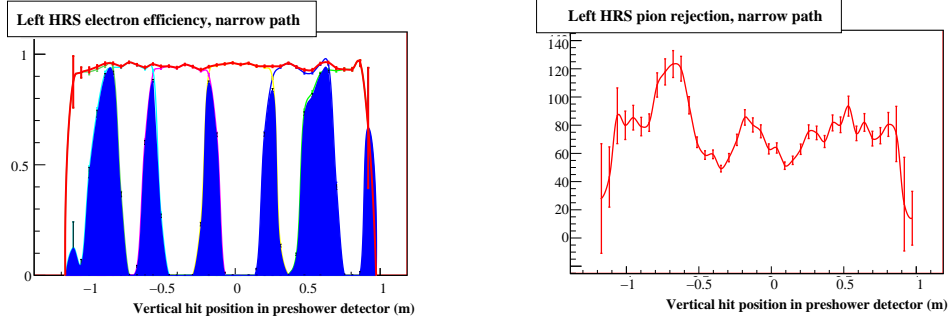


Fig. 4. [Color online] Electron detection efficiency (left) and pion rejection factor (right) vs. vertical (dispersive) hit position of the particle in the preshower detector for the narrow electron triggers in the Left HRS. A one-hour run was used in this evaluation. For electron efficiencies, the total efficiency is shown by the red curve, while blue shaded area indicates events that are recorded by the two adjacent groups. The average electron efficiency across the detector for this one-hour run is $(94.626 \pm 0.002)\%$ and the average pion rejection factor is 75.3 ± 1.1 . The error bars are statistical only. PID performance for the wide path and the Right HRS are similar.

186 4 DAQ Deadtime Study

187 Deadtime is the amount of time after an event during which the system is unable
 188 to record another event. Identifying the exact width of the deadtime is always a
 189 challenge in counting experiments. By having a narrow and wide path, we can
 190 observe the trend in the deadtime – the wider path should have higher deadtime. By
 191 matching the observed trend with our simulation we can benchmark and confirm
 192 the simulation of our deadtime. In addition, dividing lead-glass blocks into groups
 193 greatly reduces the deadtime loss in each group compared to summing all blocks
 194 together and forming only one final trigger.

195 To illustrate the importance of the deadtime, consider its affect on the asymmetry
 196 A . For a simple system with only one contribution to the deadtime δ , the observed
 197 asymmetry A_O is related to the true asymmetry A according to $A_O = (1 - \delta)A$. In
 198 our experiment δ was on the order of 0.02 (dependent on the rate), so if we want to
 199 know A with 3% accuracy, the goal is to know δ with a $\leq 30\%$ relative accuracy, so
 200 that it becomes a negligible systematic error. The DAQ we deployed was, however,
 201 more complex, having the three contributions to the deadtime, as listed below and
 202 shown in Fig. 2:

- (1) The “group” deadtime: deadtime due to discriminators and logical AND modules used to form group triggers;
- (2) The “veto” deadtime: deadtime from electronics that used scintillator and cherenkov signals to form the “gate” signals which were sent to the AND module of each group to form group electron and pion triggers.
- (3) The “OR” deadtime: deadtime due to the logical OR module when combining all group triggers.

The final deadtime is a combination of all three. In order to evaluate the DAQ deadtime, a full-scale simulation was developed as follows: The analog signals for preshower, shower, scintillator and gas cherenkov as recorded by ADCs from low-current runs are fed into the simulation as inputs. The simulation takes into account all electronics and delay cables of the DAQ and calculate digital outputs from discriminators, all AND and OR modules. For the preshower and shower SUM8 outputs, FADC data were used to determine the signal width.

4.1 Group Deadtime Measurement

In order to study the group deadtime, a high rate pulser signal (“tagger”) was mixed with all preshower and total shower signals using analog summing modules, see Figs. 2 and 5. In the absence of all detector signals, a tagger pulse produces without loss an electron trigger output, and a “tagger-trigger coincidence” pulse between this output and the delayed tagger – the tagger itself with an appropriate delay to account for the DAQ response time. When high-rate detector signals are present, however, some of the tagger would not be able to trigger the DAQ due to deadtime. The relative loss in the tagger output w.r.t. the tagger input has two components:

- (1) The count loss R_o/R_i : when a detector PMT signal precedes the tagger signal by a time interval δt shorter than the DAQ deadtime but longer than the delayed tagger pulse width, the tagger signal is lost and no coincidence output is formed;
- (2) The pileup fraction p : when a PMT signal precedes the tagger signal by a time interval δt shorter than the delayed tagger signal width, there would be coincidence output between the delayed tagger and the electron output triggered by the detector PMT signal. If δt is less than the DAQ deadtime (which is true for this experiment), the tagger itself is lost due to deadtime and the tagger-trigger coincidence is a false count and should be subtracted. In the case if δt is longer than the DAQ deadtime (not true for this experiment but could happen in general), the tagger itself also triggers a tagger-trigger coincidence but in this case, there are two tagger-trigger coincidence events, both recorded by the fbTDC if working in the multi-hit mode, and one is a false count and should be subtracted.

The pileup effect can be measured because the delay between the coinci-

dence output and the input tagger would be smaller than when the electron output is caused by the tagger. This effect is illustrated in Fig. 5 and contributes to both I_1 and I_2 region of the fbTDC spectrum. Fractions of I_1 and I_2 relative to I_0 are expected to be $I_1/I_0 = Rt_1$ and $I_2/I_0 = Rw$, respectively, where R is the PMT signal rate, w is the width of the trigger output and t_1 is the time interval the delayed tagger precedes the tagger's own trigger output. During the experiment w was set to 15 ns for all groups, t_1 was measured at the end of the experiment and was found to be between 20 and 40 ns. Data for $I_{1,2}$ extracted from fbTDC agree very well with the expected values.

The fractional loss of tagger events due to DAQ deadtime is evaluated as

$$D = 1 - (1 - p)(R_o/R_i), \quad (6)$$

where R_i is the input tagger rate, R_o is the output tagger-trigger coincidence rate, and $p = (I_1 + I_2)/I_0$ is a correction factor for pileup effects (see Fig. 5 for definition of $I_{0,1,2}$). The pileup effect was measured using fbTDC spectrum for electron narrow and wide triggers for all groups. Results for the deadtime loss D are shown in Figs. 6 and 7 and compared with simulation. Different beam currents between 20 and 100 μA were used in this dedicated deadtime measurement. In order to reduce the statistical fluctuation caused by limited number of trials in the simulation within a realistic computing time, simulations were done at higher rates than the actual measurement.

The slope of the tagger loss vs. event rate gives the value of group deadtime in seconds, as shown in Figs. 6 and 7, for group 4 on the left HRS and group 4 on the right HRS, respectively. These data are compared with results from the simulation. One can see that the deadtime for the wide path is approximately 100 ns as expected. The deadtime for the narrow path, on the other hand, is dominated by the input PMT signal width (typically 60-80 ns) instead of the 30-ns discriminator width. The simulated deadtime agree very well than data for both HRSs and for both wide and narrow paths.

4.2 Total Deadtime Evaluation

Although the deadtime loss of each group was measured using tagger signals, the dominating term in the total deadtime is from the veto electronics because the total trigger rate from scintillators and gas cherenkov is much higher than individual group rates. The difference in total loss between narrow and wide path is thus smaller than that in their group deadtimes. Simulation for the veto deadtime was compared with FADC data and the agreement was found to be at 20% level or better. After subtracting group and veto deadtimes from the total simulated deadtime, the remaining is attributed to the logical OR module. There is no direct measurement of the logical OR deadtime, but the effect of the logical OR module is quite

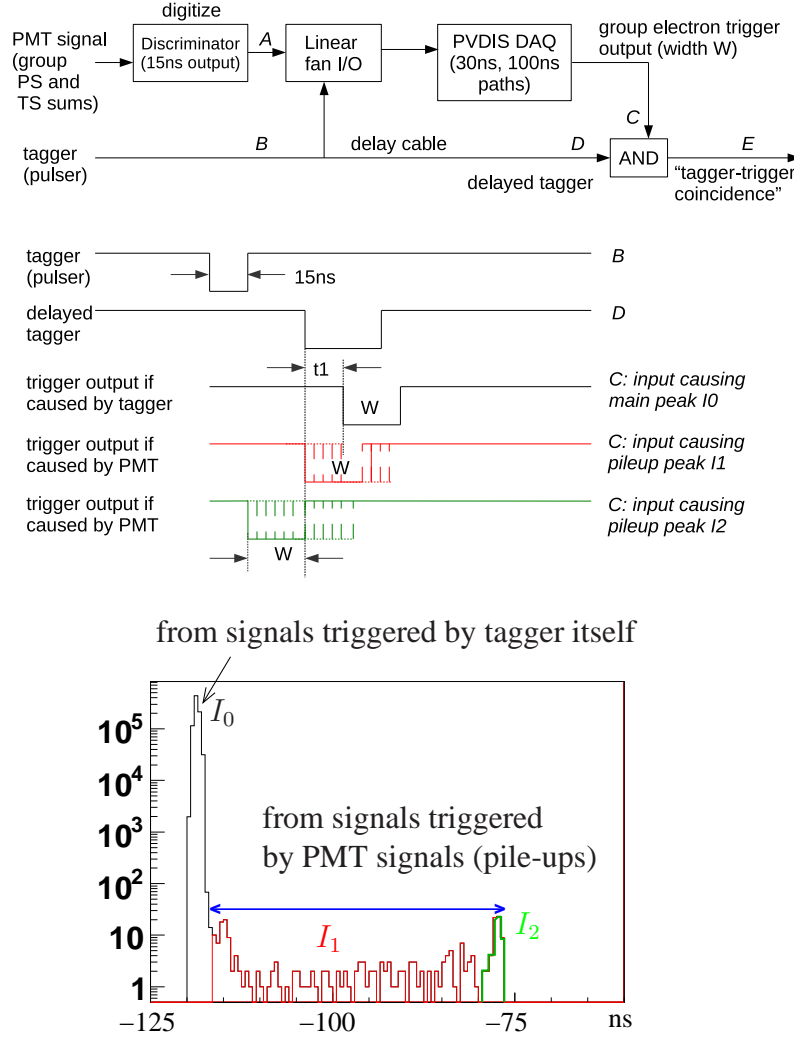


Fig. 5. [Color online] Top: schematic diagram for the tagger setup and signal timing sequence. Bottom: fbTDC spectrum for the relative timing between tagger-trigger coincidence and the input tagger, in 0.5-ns bins. The fbTDC module works in the multi-hit mode. Two different scenarios are shown: 1) Main peak I_0 : when there is no PMT signal preceding the tagger, the tagger triggers the DAQ and forms a tagger-trigger coincidence. 2) Pileup events I_1 and I_2 : when there is a PMT signal preceding the tagger by a time interval shorter than the delayed tagger width, the PMT signal triggers the DAQ and forms a tagger-trigger coincidence signal with the delayed tagger.

straightforward and can be calculated analytically. The difference between the simulation and the analytic results can be used to estimate the uncertainty of the OR

The simulated deadtime loss of the global electron triggers and its decomposition into group, veto, and OR are shown in Table 1. The total deadtime is also shown in Fig. 8 as a function of the total event rate. The deadtime corrections to

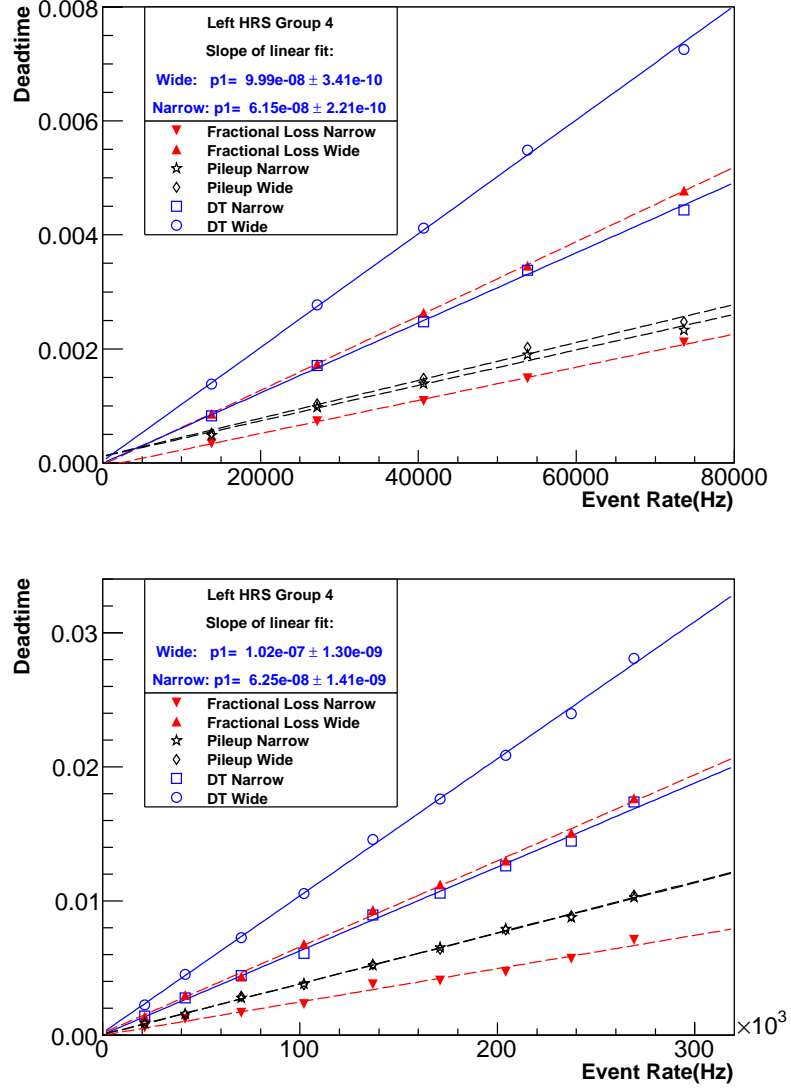


Fig. 6. [Color online] Deadtime loss in percent vs. event rate from the tagger method for group 4 on the Left HRS. Top: actual deadtime loss from tagger measurements; Bottom: simulated deadtime loss of the tagger. The tagger fractional count loss $1 - R_o/R_i$ (red) and the pileup correction p (black) are combined to form the total group deadtime D (blue). Results of the linear fit slope coefficient p_1 shows the measured or simulated group deadtime in seconds. These data were taken (or simulated) at a Q^2 of 1.1 (GeV/c)². Group 4 is from the central blocks of the lead-glass counter and has the highest rate among all groups.

the final asymmetry results from the wide path triggers are $(1.64 \pm 0.16)\%$ and $(0.931 \pm 0.215)\%$, for $Q^2 = 1.1$ and 1.9 (GeV/c)², respectively. These provide a direct correction to the measured asymmetry and the uncertainties are smaller than the 30% limit originally designed for this experiment.

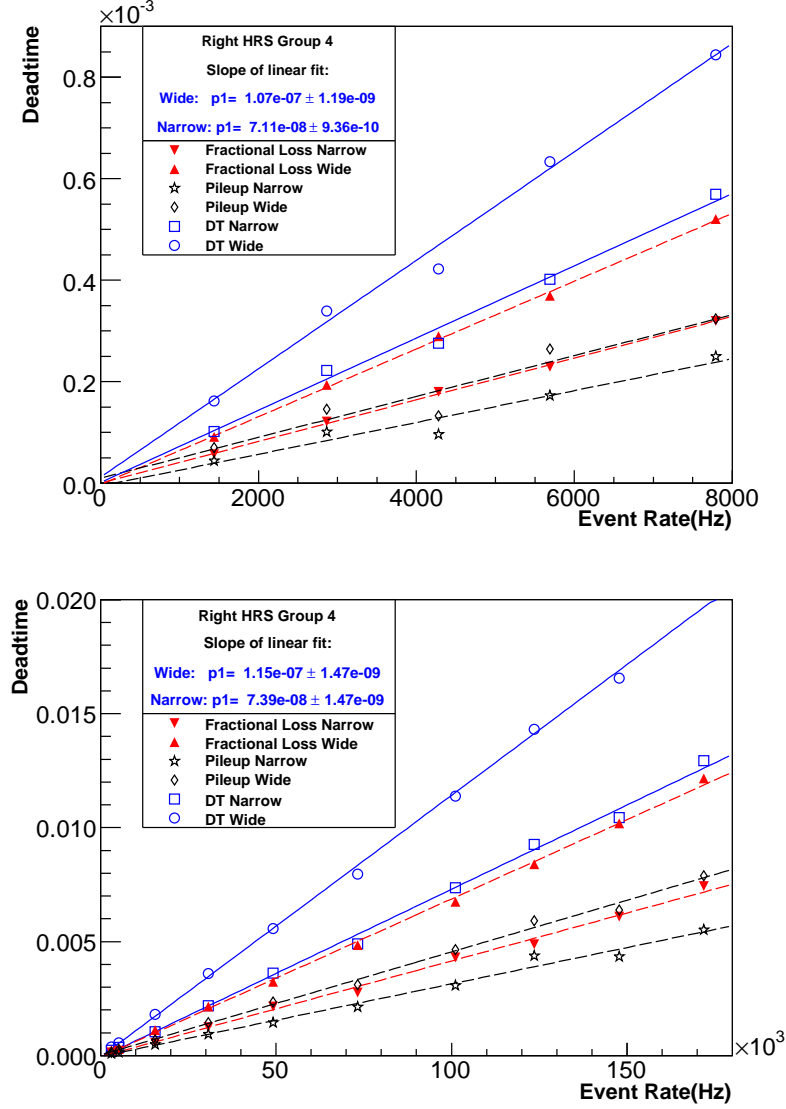


Fig. 7. [Color online] Deadtime loss in percent vs. event rate from the tagger method for group 4 on the Right HRS. Top: tagger data; Bottom: simulation. These data were taken (or simulated) at a Q^2 of 1.9 (GeV/c) 2 . Group 4 is from the central blocks of the lead-glass counter and has the highest rate among all groups. See Fig. 6 caption for details.

288 4.3 Asymmetries

289 The physics asymmetries sought for in this experiment are 90 and 160 ppm, for
 290 the two Q^2 values, respectively. The measured asymmetries are about 10% smaller
 291 due to beam polarization. To understand the systematics of the asymmetry mea-
 292 surement, a half-wave plate (HWP) was inserted in the beamline to flip the laser
 293 helicity in the polarized source during half of the data taking period. The measured
 294 asymmetries flip sign for each beam HWP change and the magnitude of the asym-
 295 metry remain consistent within statistical error bars.

Table 1

Simulated DAQ deadtime loss (in percent) and fractional contributions from group, veto, and OR deadtimes. The fractional deadtime from OR is calculated as one minus those from group and veto, and its uncertainty is estimated from the difference between simulation and the analytical results. The uncertainty of the total deadtime is the uncertainties from group, veto and OR added in quadrature.

Q^2 (GeV) ²	Path	fractional contribution			Total deadtime loss at 100 μ A
		Group	Veto	OR	
1.1	narrow	(20.6 \pm 2.1)%	(51.3 \pm 1.9)%	(28.1 \pm 8.6)%	(1.45 \pm 0.13)%
	wide	(29.5 \pm 2.4)%	(45.3 \pm 1.7)%	(25.3 \pm 9.0)%	(1.64 \pm 0.16)%
1.9	narrow	(2.9 \pm 0.2)%	(80.6 \pm 18.5)%	(16.5 \pm 12.3)%	(0.885 \pm 0.196)%
	wide	(4.3 \pm 0.4)%	(76.6 \pm 17.5)%	(19.1 \pm 15.1)%	(0.931 \pm 0.215)%

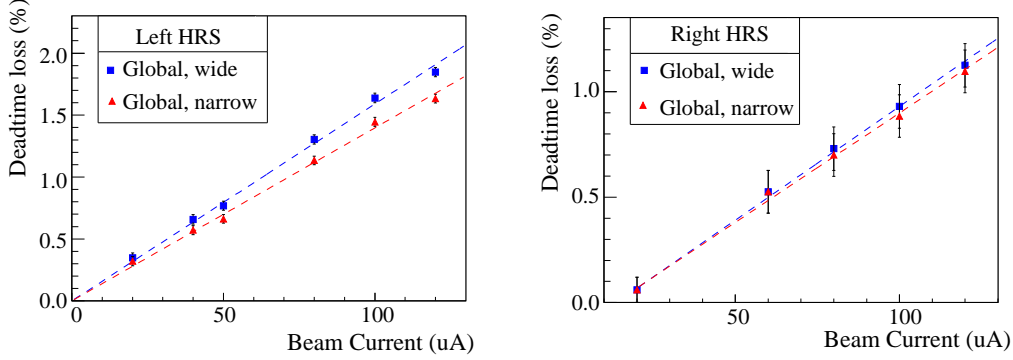


Fig. 8. [Color online] Simulated deadtime loss of the global electron trigger for the Left (left) and the Right (right) HRS. The error bars shown are due to statistical uncertainty of the simulation. See Table 1 for final uncertainty evaluation.

296 The asymmetries can be formed from event counts of each beam helicity pair,
 297 with 33-ms of helicity right and 33-ms of helicity left beam, normalized by the
 298 beam charge. Figure 9 shows the pull distribution of pair-wise asymmetries with
 299 the “pull” defined as

$$p_i \equiv (A_i - \langle A \rangle) / \delta A_i, \quad (7)$$

300 where A_i is the asymmetry extracted from the i -th beam helicity pair with the HWP
 301 states already corrected and $\delta A_i = 1 / \sqrt{N_i^R + N_i^L}$ its statistical uncertainty with
 302 $N_i^{R(L)}$ the event counts from the right (left) helicity pulse of the pair, and $\langle A \rangle$ is the
 303 asymmetry averaged over all beam pairs. One can see that the asymmetry spectrum
 304 agrees to five orders of magnitude with Gaussian distribution expected from purely
 305 statistical fluctuations.

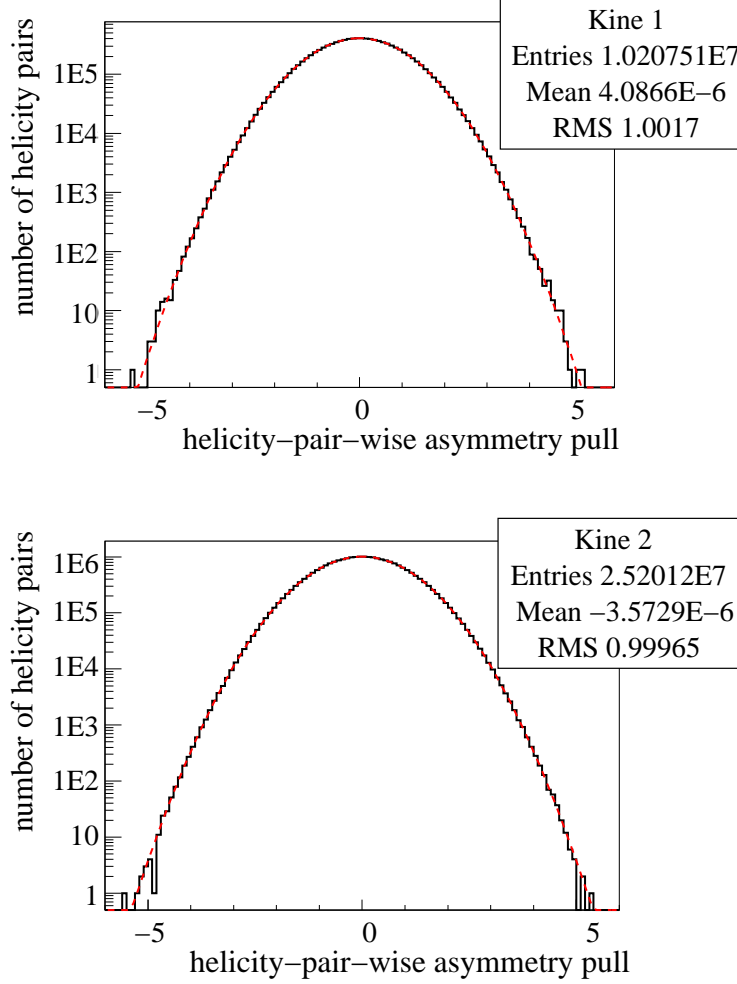


Fig. 9. [Color online] Pull distribution [Eq.(7)] for the global electron narrow trigger for $Q^2 = 1.1$ (top) and $Q^2 = 1.9$ (GeV/c)² (bottom).

5 Summary

A scaler-based counting DAQ with hardware-based particle identification was successfully implemented in the 6 GeV PVDIS experiment at Jefferson Lab. Asymmetries measured by the DAQ follow Gaussian distributions as expected from purely statistical measurements. Particle identification performance of the DAQ were measured during the experiment and corrections are applied to the data on a day-to-day basis. DAQ deadtime was calculated from a full-scale timing simulation and results are well understood. Systematic uncertainties from the new DAQ contribute to $\approx 0.2\%$ to the final asymmetry results and are negligible compared to the (3 – 4)% statistical uncertainty and other leading systematic uncertainties.

316 Acknowledgments

317 This work is supported in part by the Jeffress Memorial Trust under Award No.
318 J-836, the U.S. National Science Foundation under Award No. 0653347, and the
319 U.S. Department of Energy under Award No. DE-SC0003885. **Notice:** Authored
320 by Jefferson Science Associates, LLC under U.S. DOE Contract No. DE-AC05-
321 06OR23177. The U.S. Government retains a non-exclusive, paid-up, irrevocable,
322 world-wide license to publish or reproduce this manuscript for U.S. Government
323 purposes.

324 References

- 325 [1] JLab experiment E08-011 (previously E05-007), R. Michaels, P.E. Reimer and X.-C.
326 Zheng, spokespersons.
- 327 [2] R. Subedi *et al.*, AIP proceedings of the 18th International Spin Physics Symposium
328 (2009) 245.
- 329 [3] J. Alcorn *et al.*, Nucl. Instrum. Meth. **A522** (2004) 294.
- 330 [4] SLAC proposal E-149 P.E. Bosted *et al.*, spokespersons.
- 331 [5] C.Y. Prescott *et al.*, Phys. Lett. **B77** (1978) 347.
- 332 [6] C.Y. Prescott *et al.*, Phys. Lett. **B84** (1979) 524.
- 333 [7] D. S. Armstrong and R. D. McKeown, arXiv:1207.5238 [nucl-ex].
- 334 [8] S. Abrahamyan, Z. Ahmed, H. Albataineh, K. Aniol, D. S. Armstrong, W. Armstrong,
335 T. Averett and B. Babineau *et al.*, Phys. Rev. Lett. **108**, 112502 (2012)
336 [arXiv:1201.2568 [nucl-ex]].
- 337 [9] Z. Ahmed *et al.* [HAPPEX Collaboration], Phys. Rev. Lett. **108**, 102001 (2012)
338 [arXiv:1107.0913 [nucl-ex]].